

Exact behavior of the energy density inside a one-dimensional oscillating cavity with a thermal state

Danilo T. Alves^a, Edney R. Granhen^{b,c}, Hector O. Silva^{a,1,*}, Mateus G. Lima^{c,d}

^a*Faculdade de Física, Universidade Federal do Pará, 66075-110, Belém, PA, Brazil*

^b*Centro Brasileiro de Pesquisas Físicas, Rua Dr. Xavier Sigaud, 150, 22290-180, Rio de Janeiro, RJ, Brazil*

^c*Faculdade de Ciências Exatas e Naturais, Universidade Federal do Pará, 68505-080, Marabá, PA, Brazil*

^d*Faculdade de Engenharia Elétrica, Universidade Federal do Pará, 66075-110, Belém, PA, Brazil*

Abstract

We investigate the exact behavior of the energy density of a real massless scalar field inside a cavity with a single moving mirror executing a resonant oscillatory law of motion, satisfying Dirichlet boundary conditions at finite temperature. Our results are compared with those found in literature through analytical approximative methods.

Keywords: Dynamical Casimir effect, Energy density, Finite temperature, Oscillating cavity

PACS: 03.70.+k, 11.10.Wx, 42.50.Lc

1. Introduction

Since the pioneering work of Moore [1] and the subsequent works published in the 70s (for instance Refs. [2, 3, 4]), the problem of particle creation from vacuum due the interaction of a quantum field with moving mirrors (dynamical Casimir effect) has been subject of intense theoretical study (for recent reviews see Refs. [5] and references therein). On the experimental side, the dynamical Casimir effect has not yet been observed, despite some experimental schemes have been proposed based on simulation of a moving mirror by changing the reflectivity of a semiconductor using laser beams [6] or, more recently, using a coplanar waveguide terminated by a superconducting quantum interference device [7].

In Ref. [1], Moore considered a real massless scalar field in a two-dimensional spacetime inside a cavity with one moving boundary imposing Dirichlet boundary conditions on the field. He obtained the field solution in terms of the so-called Moore's equation. Exact analytical solutions for particular laws of motion of the boundary [8], and also approximative analytical solutions [9, 10] for the Moore's equation were obtained but, so far, there is no general technique to find analytical solutions for it. On the other hand, Cole and Schieve developed a geometrical approach to solve numerically and exactly Moore's equation [11], obtaining the exact behavior of the energy density in a non-stationary cavity considering vacuum as the initial field state [11, 12]. The dynamical Casimir effect was also studied with different approaches from that adopted by Moore, via perturbative methods for a single mirror [13] and for an oscillating cavity [14].

The quantum problem of moving mirrors with initial field states different from vacuum was also analyzed [3, 15, 16, 17, 18]. Specifically, a thermal bath was investigated for the case of a single mirror [15], and also for an oscillating cavity [16, 18]. In a recent paper [19], the present authors investigated the behavior of the energy density inside a cavity with a moving mirror, for an arbitrary initial field state, obtaining formulas which enabled us to get exact numerical results for the quantum radiation force and for the energy density in a non-static cavity for an arbitrary initial field state and law of motion for the moving boundary. However, in Ref. [19] we applied our formulas only to

*Corresponding author

Email addresses: danilo@ufpa.br (Danilo T. Alves), edney@ufpa.br (Edney R. Granhen), hosilva@ufpa.br (Hector O. Silva), mateus1@ufpa.br (Mateus G. Lima)

¹Tel/Fax: +55 91 3201-7430 (Brazil)

the case of an expanding cavity, with a non-oscillating movement and relativistic velocities. In the present letter, we consider the exact approach developed in Ref. [19] to study the behavior of the energy density for a non-static cavity with a thermal bath and a resonant oscillatory law of motion. We compare our results with those found by Andreatta and Dodonov in Ref. [18] where this problem was investigated through analytical approximative methods for small oscillations. We show the limitations in the results obtained via this approach as the amplitude of oscillation grows to outside the small oscillations regime. We also investigate the energy density outside this regime for the first time. Additionally, we show that for small amplitudes of oscillation our results are in excellent agreement with [18].

This Letter is organized as follows: in Sec. 2 we obtain the field solution and the exact formulas for the energy density taking the initial field state as a thermal bath and considering that the mirrors impose Dirichlet boundary condition on the field. In Sec. 3 we study the behavior of the energy density for the case of an oscillatory law of motion for the moving boundary. Finally, in Sec. 4 we summarize our results.

2. Exact formulas for the energy density

Let us start considering the real massless scalar field satisfying the Klein-Gordon equation (we assume throughout this paper $\hbar = c = k_B = 1$): $(\partial_t^2 - \partial_x^2)\psi(t, x) = 0$, and obeying Dirichlet boundary conditions imposed at the static boundary located at $x = 0$, and also at the moving boundary's position at $x = L(t)$, that is $\psi(t, 0) = \psi(t, L(t)) = 0$, where $L(t)$ is an arbitrary prescribed law for the moving boundary with $L(t \leq 0) = L_0$, with L_0 being the length of the cavity in the static situation.

The field in the cavity can be obtained by exploiting the conformal invariance of the Klein-Gordon equation [1, 2]. The field operator, solution of the wave equation, can be written as:

$$\hat{\psi}(t, x) = \sum_{n=1}^{\infty} [\hat{a}_n \psi_n(t, x) + H.c.], \quad (1)$$

where the field modes $\psi_n(t, x)$ are given by:

$$\psi_n(t, x) = \frac{1}{\sqrt{4n\pi}} [\varphi_n(v) + \varphi_n(u)], \quad (2)$$

with $\varphi_n(z) = \exp[-in\pi R(z)]$, $u = t - x$, $v = t + x$. The function R satisfies Moore's equation:

$$R[t + L(t)] - R[t - L(t)] = 2. \quad (3)$$

Considering the Heisenberg picture, we are interested in the averages $\langle \dots \rangle$ taken over a thermal state. For this particular field state we have $\langle \hat{a}_n^\dagger \hat{a}_{n'} \rangle = \delta_{nn'} \xi_n(T)$ and $\langle \hat{a}_n \hat{a}_{n'} \rangle = \langle \hat{a}_n^\dagger \hat{a}_{n'}^\dagger \rangle = 0$, where $\xi_n(T) = \{\exp[n\pi/(L_0 T)] - 1\}^{-1}$ and T is the temperature.

Taking the expected value of the energy density operator $\mathcal{T} = \langle \hat{T}_{00}(t, x) \rangle$, where [2]

$$\hat{T}_{00}(t, x) = \frac{1}{2} \left[\left(\frac{\partial \hat{\psi}}{\partial t} \right)^2 + \left(\frac{\partial \hat{\psi}}{\partial x} \right)^2 \right], \quad (4)$$

we can split the renormalized energy density \mathcal{T} as follows [19]:

$$\mathcal{T} = \mathcal{T}_{\text{vac}} + \mathcal{T}_{\text{non-vac}}, \quad (5)$$

where

$$\mathcal{T}_{\text{vac}} = -f(v) - f(u), \quad (6)$$

$$\mathcal{T}_{\text{non-vac}} = -g(v) - g(u), \quad (7)$$

with

$$g(z) = -\frac{\pi}{2} \sum_{n=1}^{\infty} n [R'(z)]^2 \xi_n(T), \quad (8)$$

$$f(z) = \frac{1}{24\pi} \left\{ \frac{R'''(z)}{R'(z)} - \frac{3}{2} \left[\frac{R''(z)}{R'(z)} \right]^2 + \frac{\pi^2}{2} R'(z)^2 \right\}. \quad (9)$$

In Eqs. (8) and (9) the derivatives, denoted by the primes, are taken with respect to the argument of the function R .

For further analysis, it is useful to write [19]:

$$\mathcal{T} = -h(v) - h(u), \quad (10)$$

where $h(z) = f(z) + g(z)$.

In the static situation $t \leq 0$, where both boundaries are at rest, the function R is given by $R(z) = z/L_0[1]$. The functions f and g , now relabeled, respectively, as $f^{(s)}$ and $g^{(s)}$, are now given by:

$$f^{(s)} = \frac{\pi}{48L_0^2}, \quad (11)$$

$$g^{(s)} = -\frac{\pi}{2L_0^2} \sum_{n=1}^{\infty} n \xi_n(T). \quad (12)$$

Note that in the static situation \mathcal{T}_{vac} is the Casimir energy density $\mathcal{T}_{\text{cas}} = -\pi/(24L_0^2)$. In Ref. [19] it was shown that the behavior of the energy density in a cavity is determined by the function h , which obeys:

$$h[t + L(t)] = h[t - L(t)] \mathcal{A}(t) + \mathcal{B}(t). \quad (13)$$

where

$$\mathcal{A}(t) = \left[\frac{1 - L'(t)}{1 + L'(t)} \right]^2, \quad (14)$$

$$\begin{aligned} \mathcal{B}(t) = & -\frac{1}{12\pi} \frac{L'''(t)}{[1 + L'(t)]^3 [1 - L'(t)]} \\ & -\frac{1}{4\pi} \frac{L''^2(t) L'(t)}{[1 + L'(t)]^4 [1 - L'(t)]^2}. \end{aligned} \quad (15)$$

Eq. (13) enables us to obtain recursively the value of $h(z)$, and consequently the energy density \mathcal{T} (10), in terms of its static value

$$h^{(s)} = f^{(s)} + g^{(s)}.$$

Solving recursively the Eq. (13), as discussed in Ref. [19] in details, we can write $h(z)$ in the following manner:

$$h(z) = h^{(s)} \tilde{\mathcal{A}}(z) + \tilde{\mathcal{B}}(z), \quad (16)$$

where:

$$\tilde{\mathcal{A}}(z) = \prod_{i=1}^{n(z)} \mathcal{A}[t_i(z)], \quad (17)$$

$$\tilde{\mathcal{B}}(z) = \sum_{j=1}^{n(z)} \mathcal{B}[t_j(z)] \prod_{i=1}^{j-1} \mathcal{A}[t_i(z)], \quad (18)$$

$$z = t_1 + L(t_1), \quad (19)$$

$$t_{i+1} + L(t_{i+1}) = t_i - L(t_i), \quad i = 1, 2, 3, \dots, \quad (20)$$

being n the number of reflections of the null lines on the moving boundary world line during the recursive process. We remark that in Eq. (16), the functions $\tilde{\mathcal{A}}$ and $\tilde{\mathcal{B}}$ depend only on the law of motion of the moving mirror, whereas

the dependence on the initial field state is stored in the static value $h^{(s)}$. We also observe that, for a generic law of motion, $\tilde{\mathcal{A}}$ and $\tilde{\mathcal{B}}$ are different functions, with the following properties [19]:

$$\tilde{\mathcal{A}}(z) > 0 \quad \forall z, \quad \tilde{\mathcal{A}}(z < L_0) = 1, \quad \tilde{\mathcal{B}}(z < L_0) = 0, \quad (21)$$

The energy densities \mathcal{T}_{vac} and $\mathcal{T}_{\text{non-vac}}$ (Eqs. (6) and (7)) are now respectively rewritten as:

$$\mathcal{T}_{\text{vac}} = -f^{(s)} [\tilde{\mathcal{A}}(u) + \tilde{\mathcal{A}}(v)] - \tilde{\mathcal{B}}(u) - \tilde{\mathcal{B}}(v), \quad (22)$$

$$\mathcal{T}_{\text{non-vac}} = -g^{(s)} [\tilde{\mathcal{A}}(u) + \tilde{\mathcal{A}}(v)]. \quad (23)$$

From Eqs. (5), (22) and (23) the exact formula for the total energy density \mathcal{T} is now given by:

$$\mathcal{T} = -h^{(s)} [\tilde{\mathcal{A}}(u) + \tilde{\mathcal{A}}(v)] - \tilde{\mathcal{B}}(u) - \tilde{\mathcal{B}}(v). \quad (24)$$

In this two-dimensional model the instantaneous force \mathcal{F} acting on the moving boundary (disregarding the contribution of the field outside the cavity) is given by $\mathcal{F}(t) = \mathcal{T}[t, L(t)]$. We also define $\mathcal{F}_{\text{vac}}(t) = \mathcal{T}_{\text{vac}}[t, L(t)]$ and $\mathcal{F}_{\text{non-vac}}(t) = \mathcal{T}_{\text{non-vac}}[t, L(t)]$.

With this results in hand, we are ready to investigate the exact behavior of the energy density for a thermal state and make comparison with the results found through the analytical approximative approach found in the literature.

3. Comparing exact and approximate results for the energy density

From Eqs. (14), (15), (17) and (18) we see that the functions $\tilde{\mathcal{A}}$ and $\tilde{\mathcal{B}}$ are different one from another for an arbitrary law of motion. Therefore, our first conclusion is that the functions \mathcal{T}_{vac} and $\mathcal{T}_{\text{non-vac}}$ (given by Eqs. (22) and (23)) consequently have, in general, different structures as well. Hereafter we use the word structure in the following sense: two graphs have the same structure if they have the same number of maximum and minimum points and these points are at the same positions in both graphs. As a direct consequence of our first conclusion, we can say that the thermal force $\mathcal{F}_{\text{non-vac}}$ and the radiation reaction force \mathcal{F}_{vac} have in general different structures. At a first glance, our conclusion contrasts with that found by Andreata and Dodonov [18], according to which \mathcal{T}_{vac} and $\mathcal{T}_{\text{non-vac}}$ exhibit a same structure for initial diagonal states (as the case of the thermal state). Next we will discuss this issue.

Let us consider the particular laws of motion given by

$$L(t) = L_0 \left[1 + \epsilon \sin \left(\frac{p\pi t}{L_0} \right) \right], \quad (25)$$

where $L_0 = 1$, $p = 1, 2, \dots$, and ϵ is a dimensionless parameter. This oscillatory boundary motion was investigated in several papers (see, for instance, Refs. [9, 18]), with the calculation of the energy density developed in the context of analytical approximative methods, considering small amplitudes of oscillation ($|\epsilon| \ll 1$). Taking as basis the results found in Ref. [18], the renormalized energy density \mathcal{T} , corresponding to the laws of motion (25) is given by $\mathcal{T} \approx \mathcal{T}^{(a)}$, with

$$\mathcal{T}^{(a)} = -(h^{(s)} - p^2 f^{(s)})[s(u) + s(v)] - 2p^2 f^{(s)}, \quad (26)$$

where:

$$\begin{aligned} s(z) &= \frac{(1 - \kappa^2)^2}{[1 + \kappa^2 + 2(-1)^p \kappa \cos(p\pi z)]^2}, \\ \kappa &= \frac{\sinh(p\tau)}{\sqrt{1 + \sinh^2(p\tau)}}, \\ \tau &= \frac{1}{2L_0} \epsilon \pi t, \end{aligned}$$

being $t = N/p$ and N a non-negative integer. The energy density $\mathcal{T}^{(a)}$ in Eq. (26) also can be written in terms of the vacuum and non-vacuum contributions as $\mathcal{T}^{(a)} = \mathcal{T}_{\text{vac}}^{(a)} + \mathcal{T}_{\text{non-vac}}^{(a)}$, where:

$$\mathcal{T}_{\text{vac}}^{(a)} = (p^2 - 1)f^{(s)}[s(u) + s(v)] - 2p^2 f^{(s)}, \quad (27)$$

$$\mathcal{T}_{\text{non-vac}}^{(a)} = -g^{(s)}[s(u) + s(v)]. \quad (28)$$

Let us focus initially on the case $p > 1$. Since $(p^2 - 1)f^{(s)} > 0$ and $-g^{(s)} > 0$, Eqs. (27) and (28) give that the functions $\mathcal{T}_{\text{vac}}^{(a)}$ and $\mathcal{T}_{\text{non-vac}}^{(a)}$ have the same structure [18]. To conciliate this conclusion with our first conclusion mentioned above, we will show next, starting from our exact approach, that we can find a class of motions for which the energy density (24) is $\mathcal{T} \approx \mathcal{T}^{(a)}$, so that \mathcal{T}_{vac} and $\mathcal{T}_{\text{non-vac}}$ exhibit approximately the same structure, and that the particular laws of motion (25) - investigated in Ref. [18] - belong to this class.

Looking for conditions under which \mathcal{T}_{vac} and $\mathcal{T}_{\text{non-vac}}$ have the same structure we find that one condition is provided by the laws of motion for which $\tilde{\mathcal{A}}(z)$ and $\tilde{\mathcal{B}}(z)$ have a linear relation of the form:

$$\tilde{\mathcal{B}}(z) = k_1 \tilde{\mathcal{A}}(z) + k_2, \quad (29)$$

where k_1 and k_2 are constants. From the properties given in Eq. (21), we get $k_1 = -k_2$, resulting in:

$$\tilde{\mathcal{B}}(z) = k_1 [\tilde{\mathcal{A}}(z) - 1], \quad (30)$$

and from Eqs. (22), (23) and (30), we have:

$$\mathcal{T}_{\text{vac}} = -\left(f^{(s)} + k_1\right) [\tilde{\mathcal{A}}(u) + \tilde{\mathcal{A}}(v)] + 2k_1, \quad (31)$$

$$\mathcal{T}_{\text{non-vac}} = -g^{(s)} [\tilde{\mathcal{A}}(u) + \tilde{\mathcal{A}}(v)], \quad (32)$$

$$\mathcal{T} = -\left(h^{(s)} + k_1\right) [\tilde{\mathcal{A}}(u) + \tilde{\mathcal{A}}(v)] + 2k_1. \quad (33)$$

Then, our second conclusion is that if the constant factors multiplying $\tilde{\mathcal{A}}(u) + \tilde{\mathcal{A}}(v)$ are different from zero and have the same sign, as the ratio

$$\sigma(z) = \frac{\tilde{\mathcal{B}}(z)}{\tilde{\mathcal{A}}(z) - 1} \quad (34)$$

becomes more close to a constant value k_1 , that means

$$\sigma(z) \approx k_1, \quad (35)$$

more the structures of the functions \mathcal{T}_{vac} and $\mathcal{T}_{\text{non-vac}}$ become similar to one another, whereas if they have different sign then where we find valleys and peaks in a graph, we can have respectively peaks and valleys in the other. As a direct consequence, for the class of motions obeying the condition (35) the quantum radiation forces \mathcal{F}_{vac} and $\mathcal{F}_{\text{non-vac}}$ also have similar structures.

Comparing our Eq. (33) with (26), we see that both have the same structure. Our third conclusion is that the formula (26) found by Andreatta and Dodonov belongs to the particular class of formulas (given by Eq. (33)) for the energy density. We will show that this occurs because for the laws of motion (25), as the condition $|\epsilon| \ll 1$ is better satisfied, better is satisfied the condition (35).

In Fig. 1, using (17) and (18), we plot the ratio σ (Eq. (34)) for $p = 2$, taking into account three values of amplitudes of oscillation: $\epsilon = 10^{-3}$, $\epsilon = 10^{-2}$ and $\epsilon = 10^{-1}$. We observe that σ is more approximately the constant value $-4f^{(s)}$ for $\epsilon = 10^{-3}$ (dash-dotted line) than for $\epsilon = 10^{-1}$ (solid line).

In Fig. 2 we plot σ for the case $p = 3$, observing that as ϵ becomes smaller σ tends to the value $-9f^{(s)}$. Then we see that, in the limit $\epsilon \rightarrow 0$ we get:

$$\sigma \rightarrow k_1 = -p^2 f^{(s)}. \quad (36)$$

In Fig. 3, we plot the ratio $\lambda(z) = \tilde{\mathcal{A}}(z)/s(z)$ for $p = 2$, taking into account the values $\epsilon = 10^{-4}$, $\epsilon = 10^{-3}$, $\epsilon = 10^{-2}$ and $\epsilon = 10^{-1}$. We observe that as $\epsilon \rightarrow 0$ we have $\lambda(z) \rightarrow 1$, what means:

$$\tilde{\mathcal{A}}(z) \rightarrow s(z). \quad (37)$$

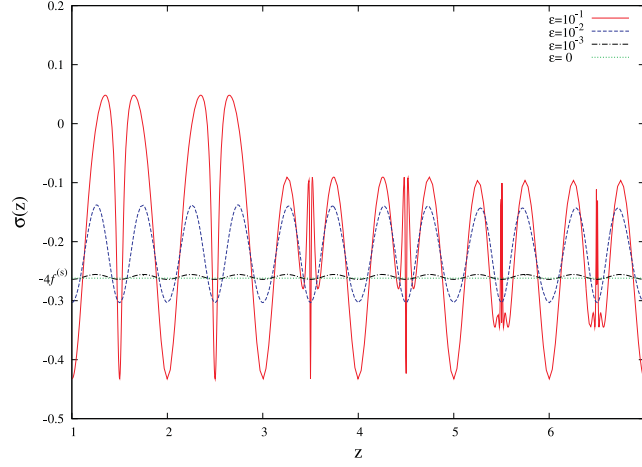


Figure 1: The ratio $\sigma(z) = \tilde{\mathcal{B}}(z)/[\tilde{\mathcal{A}}(z) - 1]$ for the law of motion given by Eq. (25) with $p = 2$. We use different scales for $\sigma(z)$ in each case. The solid line corresponds to the case $\epsilon = 10^{-1}$. The dashed line corresponds to the case $\epsilon = 10^{-2}$, exhibiting $40 \times [\sigma(z) + 4f^{(s)}] - 4f^{(s)}$. The dash-dotted line corresponds to the case $\epsilon = 10^{-3}$, showing $200 \times [\sigma(z) + 4f^{(s)}] - 4f^{(s)}$. The dotted line corresponds to the case $\epsilon = 0$. As $\epsilon \rightarrow 0$ we have $\sigma(z) \rightarrow -4f^{(s)}$.

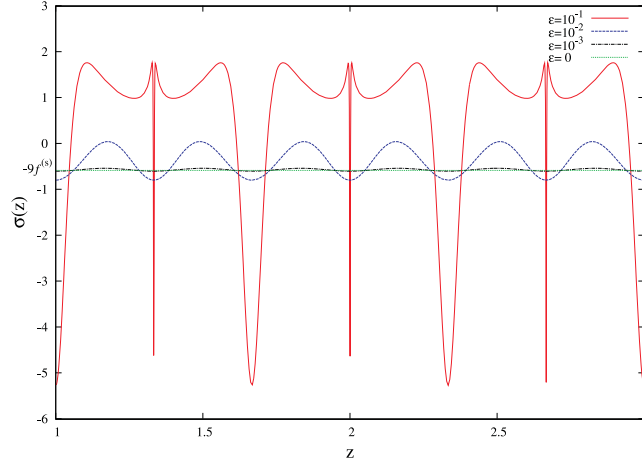


Figure 2: The ratio $\sigma(z) = \tilde{\mathcal{B}}(z)/[\tilde{\mathcal{A}}(z) - 1]$ for the law of motion given by Eq. (25) with $p = 3$. We use different scales for $\sigma(z)$ in each case. The solid line corresponds to the case $\epsilon = 10^{-1}$. The dashed line corresponds to the case $\epsilon = 10^{-2}$, exhibiting $40 \times [\sigma(z) + 9f^{(s)}] - 9f^{(s)}$. The dash-dotted line corresponds to the case $\epsilon = 10^{-3}$, showing $300 \times [\sigma(z) + 9f^{(s)}] - 9f^{(s)}$. The dotted line corresponds to the case $\epsilon = 0$. As $\epsilon \rightarrow 0$ we have $\sigma(z) \rightarrow -9f^{(s)}$.

Eqs. (36) and (37) complete the mapping between Eqs. (33) and (26), demonstrating a perfect agreement between two completely different approaches to the problem

Now, let us investigate the following point: since Eqs. (27) and (28) are approximations, we should find differences between the structures of the vacuum and non-vacuum parts when we consider the case of the law of motion (25) with our exact approach. To investigate this issue, we study the law of motion (25) for $\epsilon = 10^{-2}$ and $\epsilon = 10^{-1}$. Our aim now is to verify, using the exact approach, the similarities and differences between the structures of \mathcal{T}_{vac} and $\mathcal{T}_{\text{non-vac}}$ for both values of ϵ .

Although the formulas (17), (18), (22) and (23) are formally exact, to extract numerical values for \mathcal{T}_{vac} and

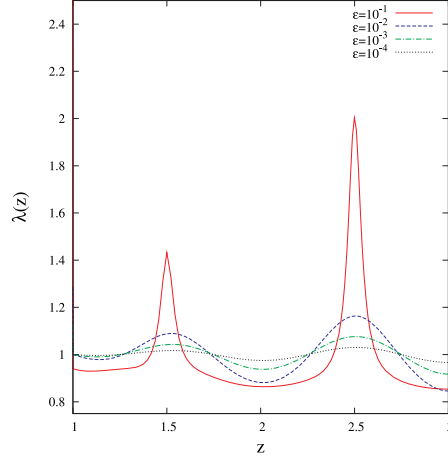


Figure 3: The ratio $\lambda(z) = \tilde{\mathcal{A}}(z)/s(z)$ for the law of motion given by Eq. (25) with $p = 2$. We use different scales for $\lambda(z)$ in each case. The solid line describes the case $\epsilon = 10^{-1}$, exhibited as $1/6 \times [\lambda(z) - 1] + 1$. The dashed line describes the case $\epsilon = 10^{-2}$. The dash-dotted line corresponds to the case $\epsilon = 10^{-3}$, exhibiting $1/5 \times \lambda(z)$, whereas the dotted line corresponds to the case $\epsilon = 10^{-4}$, showing $20 \times \lambda(z)$. As $\epsilon \rightarrow 0$ we have $\lambda(z) \rightarrow 1$.

$\mathcal{T}_{\text{non-vac}}$ we need to calculate the functions $t_i(z)$, which are given by Eqs. (19) and (20). For the law of motion (25) (and in general) we can get only numerical solutions of (19) and (20). For a given value of z , the Eq. (19) can be solved numerically and the result for t_1 naturally has a certain limited accuracy. When t_1 is used in Eq. (20) to calculate t_2 , the solution of $t_2 + L(t_2) = t_1 - L(t_1)$ can give a result less accurate than the result previously obtained for t_1 , and successive calculations of the remaining values of t_i via equations (20) (for $i = 2, 3, 4, \dots$) could generate a final result for t_n with a poor accuracy, if compared to the accuracy of the initial value for t_1 . Moreover, when we insert the numerical values for t_i in Eqs. (17), (18), (22) and (23), the final values for \mathcal{T}_{vac} and $\mathcal{T}_{\text{non-vac}}$ could have their accuracy diminished even more. To deal with this question and control the final accuracy of our results, we perform the numerical calculations in Maple computer algebra system [20], which enables us to control the number of digits used when calculating with floating-point numbers. To obtain a final numerical value for \mathcal{T}_{vac} or $\mathcal{T}_{\text{non-vac}}$, we carry out several independent calculations using our routines developed in Maple [21]. In each calculation we take all numerical solutions with a certain number of digits. Considering from 3 to 100 digits, we observe the convergence of the results as the number of digits (related to the initial accuracy considered for the solution of (19)) is enhanced. This enable us to point which are the exact digits (the accuracy) in our results. For instance, the values of $\mathcal{T}_{\text{vac}}(10, 0.5)$ ($L_0 = 1, p = 2$) performed with 3, 4, 5, 6, 10 and 20 digits are given, respectively by: 0.856, 0.8638, 0.86364, 0.863704, 0.8637005768 and 0.86370057587773139184. Analyzing also the convergence of the results up to 100 digits, we can obtain a final accuracy of 10 or more digits, but we just display the result as $\mathcal{T}_{\text{vac}}(10, 0.5) \approx 0.864$, where the first two digits can be considered as exact digits. Hereafter, the exhibited results have accuracy at least up to the penultimate digit shown.

In Fig. 4, using the formulas (22) and (23) we plot the energy densities \mathcal{T}_{vac} and $\mathcal{T}_{\text{non-vac}}$ for the case $p = 2, T = 1, \epsilon = 10^{-2}$ at $t = 20.2$. We see that both energy densities have two peaks (in this case, located at $x = 0.30$ and $x = 0.70$, with values $\mathcal{T}_{\text{vac}}(20.2, 0.30) = \mathcal{T}_{\text{vac}}(20.2, 0.70) \approx 1.94$ and $\mathcal{T}_{\text{non-vac}}(20.2, 0.30) = \mathcal{T}_{\text{non-vac}}(20.2, 0.70) \approx 23.3$), both have three minimum points (located at $x = 0, x = 0.50, x = 1.01$, with values $\mathcal{T}_{\text{vac}}(20.2, 0) \approx -0.453, \mathcal{T}_{\text{vac}}(20.2, 0.5) \approx -0.322, \mathcal{T}_{\text{vac}}(20.2, 1.01) \approx -0.461, \mathcal{T}_{\text{non-vac}}(20.2, 0) \approx 0.647, \mathcal{T}_{\text{non-vac}}(20.2, 0.5) \approx 1.9, \mathcal{T}_{\text{non-vac}}(20.2, 1.01) \approx 0.579$), so that \mathcal{T}_{vac} and $\mathcal{T}_{\text{non-vac}}$ exhibit the same structure, as predicted by the approximate analytical formulas (27) and (28) [18], which are based on the assumption $|\epsilon| \ll 1$. We remark that $x \approx 1.01$ corresponds to the position of the right mirror when $t = 20.2$ ($L(20.2) \approx 1.01$).

For the case $\epsilon = 10^{-1}$, we get for $\mathcal{T}_{\text{vac}}(20.2, x)$ and $\mathcal{T}_{\text{non-vac}}(20.2, x)$ that both present again two narrow peaks, located at $x = 0.30$ and $x = 0.70$ (similarly to the case showed in Fig. 4, but with values $\mathcal{T}_{\text{vac}}(20.2, 0.30) = \mathcal{T}_{\text{vac}}(20.2, 0.70) \approx 0.249 \times 10^{13}$, $\mathcal{T}_{\text{non-vac}}(20.2, 0.30) = \mathcal{T}_{\text{non-vac}}(20.2, 0.70) \approx 0.126 \times 10^{14}$). Moreover, in the

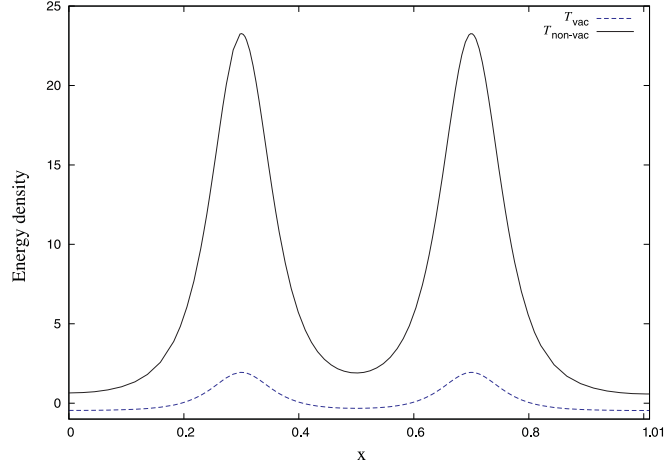


Figure 4: The energy densities \mathcal{T}_{vac} (dashed line) and $\mathcal{T}_{\text{non-vac}}$ (solid line) at the instant $t = 20.2$ with $T = 1$, plotted via the exact formulas (22) and (23). We consider the law of motion (25) with $p = 2$ and $\epsilon = 10^{-2}$.

case $\epsilon = 10^{-1}$, $\mathcal{T}_{\text{vac}}(20.2, x)$ exhibits several other maximum and minimum points that are not visualized in the graph of $\mathcal{T}_{\text{non-vac}}(20.2, x)$.

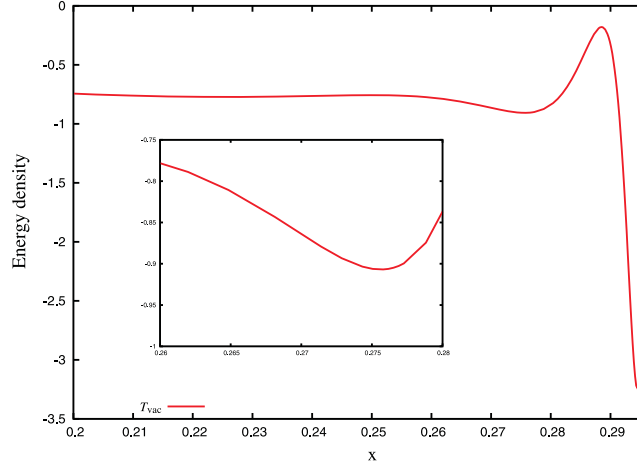


Figure 5: Detail of the energy density \mathcal{T}_{vac} at the instant $t = 20.2$, for the law of motion (25) with $p = 2$, $T = 1$ and $\epsilon = 10^{-1}$, plotted via the exact formula (22) in the region $0.2 < x < 0.3$. In detail we show \mathcal{T}_{vac} in the sub-region $0.26 < x < 0.28$. The spacing used between the calculated points in the graph is 10^{-4} .

In Fig. 5 we investigate details of the behavior of \mathcal{T}_{vac} for the case $\epsilon = 10^{-1}$ in the region $0.2 < x < 0.3$. We can see peaks for the following values: $x \approx 0.250$ and $x \approx 0.289$; we also see minimum values at the points $x \approx 0.230$, $x \approx 0.28$ and $x \approx 0.295$.

In Fig. 6 we see the behavior of $\mathcal{T}_{\text{non-vac}}$ (for $\epsilon = 10^{-1}$ and $T = 1$), in the same region as Fig. 5, but there is no peak or valley. Then we verify that when we consider $\epsilon = 10^{-2}$ and $\epsilon = 10^{-1}$, since the former value is in better agreement with the conditions $|\epsilon| \ll 1$ and $\sigma \approx -p^2 f^{(s)} = -4\pi$, no difference between the structures of \mathcal{T}_{vac} and $\mathcal{T}_{\text{non-vac}}$ is perceived, but for the latter value of ϵ differences between the structures of \mathcal{T}_{vac} (Fig. 6) and $\mathcal{T}_{\text{non-vac}}$ (Fig. 5) become evident, as predicted via the exact formulas (22) and (23).

For $p = 1$, Eq. (27) gives $\mathcal{T}_{\text{vac}} \approx \mathcal{T}_{\text{vac}}^{(a)} = -2f^{(s)} = \mathcal{T}_{\text{cas}}$, so that the energy density would conserve its vacuum

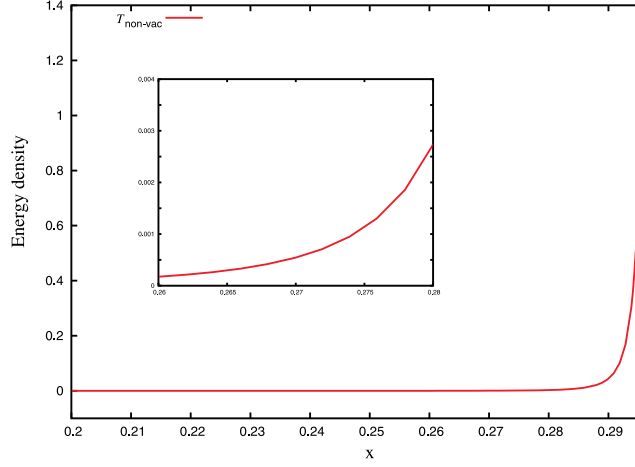


Figure 6: The energy density $\mathcal{T}_{\text{non-vac}}$ at the instant $t = 20.2$, for the law of motion (25) with $p = 2$ and $\epsilon = 10^{-1}$, plotted via the exact formula (23) in the region $0.2 < x < 0.3$. In detail we show $\mathcal{T}_{\text{non-vac}}$ in the sub-region $0.26 < x < 0.28$. The spacing used between the calculated points in the graph is 10^{-4} .

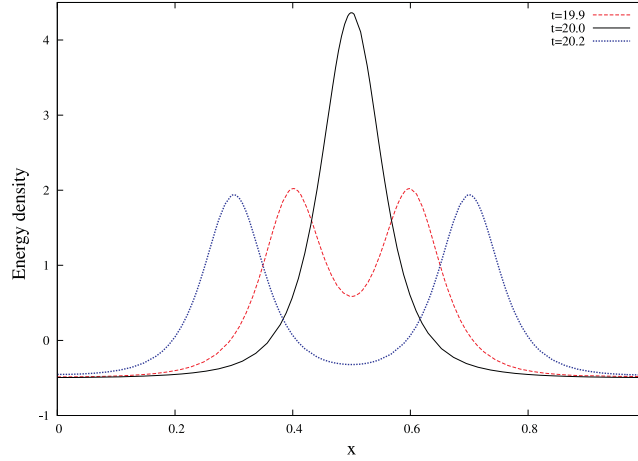


Figure 7: The time evolution of the energy density \mathcal{T}_{vac} for the law of motion (25), with $p = 2$ and $\epsilon = 10^{-2}$, plotted via the exact formula (22). The dashed line shows two peaks at $t = 19.9$, initializing the merging process. The solid line shows the maximum peak formed at $x = 0.5$ and $t = 20$. The dotted line shows the energy density at $t = 20.2$, after the merging.

(Casimir) value, whereas Eq. (28) gives for $\mathcal{T}_{\text{non-vac}}^{(a)}$ a spacetime dependence. However, the exact behavior is given by Eqs. (22) and (23), which show that the values of both \mathcal{T}_{vac} and $\mathcal{T}_{\text{non-vac}}$ change in time and space. For instance, for the law of motion (25) with $p = 1$ and $\epsilon = 10^{-2}$, the exact behavior of $\mathcal{T}_{\text{vac}}^{(a)}(100.5, x)$ exhibits two minimum points surrounding a peak located at $x = 0.5$ (see also Ref. [11]), whereas $\mathcal{T}_{\text{non-vac}}^{(a)}(100.5, x)$ displays a peak at $x = 0.5$. For this case $p = 1$, Eq. (36) remains valid, so that as $\epsilon \rightarrow 0$, $\mathcal{T}_{\text{vac}}^{(a)}$ and $\mathcal{T}_{\text{non-vac}}^{(a)}$ display more similar structures.

Now, we will compare exact and approximate results in the prediction of the maximum value of the peaks in the energy density moving in an oscillating cavity. In this context, let us analyze again the behavior of $\mathcal{T}_{\text{vac}}(t, x)$ and $\mathcal{T}_{\text{non-vac}}(t, x)$ for the case $p = 2$. The two peaks showed in Fig. 4 (for $\mathcal{T}_{\text{vac}}(t, x)$ or $\mathcal{T}_{\text{non-vac}}(t, x)$) have the same value (see values presented above), move in opposite direction and at $(t, x) = (N, 0.5)$ (N is a non-negative integer) they merge forming a single maximum peak (see Fig. 7). The maximum value of the energy density occurs when the

two peaks merge. This value is represented for vacuum and non-vacuum parts, respectively, by $\mathcal{T}_{\text{vac}}^{\text{max}}$ and $\mathcal{T}_{\text{non-vac}}^{\text{max}}$. Exactly, we have

$$\mathcal{T}_{\text{vac}}^{\text{max}} = \mathcal{T}_{\text{vac}}(N, 0.5), \quad (38)$$

$$\mathcal{T}_{\text{non-vac}}^{\text{max}} = \mathcal{T}_{\text{non-vac}}(N, 0.5). \quad (39)$$

From an approximate analysis, taking as basis the results found in Ref. [18], $\mathcal{T}_{\text{vac}}^{\text{max}}$ and $\mathcal{T}_{\text{vac}}^{\text{max}}$ grow in time according to $\mathcal{T}_{\text{vac}}^{\text{max}} \approx \mathcal{T}_{\text{vac}}^{(a)\text{max}}$ and $\mathcal{T}_{\text{non-vac}}^{\text{max}} \approx \mathcal{T}_{\text{non-vac}}^{(a)\text{max}}$, where

$$\mathcal{T}_{\text{vac}}^{(a)\text{max}} = 6f^{(s)}(e^{8\tau} - 1) - 2f^{(s)}, \quad (40)$$

$$\mathcal{T}_{\text{non-vac}}^{(a)\text{max}} = -2g^{(s)} \frac{(1 + \kappa)^2}{(1 - \kappa)^2}. \quad (41)$$

In Fig. 8 we examine the case given by the law of motion (25), $p = 2$ and $\epsilon = 10^{-2}$, and visualize agreement between the growing in time of the peaks predicted by the approximate formula (40) and the exact values obtained via (38). In Table 1, again considering $\epsilon = 10^{-2}$, we compare $\mathcal{T}_{\text{vac}}^{\text{max}}$ with $\mathcal{T}_{\text{vac}}^{(a)\text{max}}$ for larger times, and also compare $\mathcal{T}_{\text{non-vac}}^{\text{max}}$ with $\mathcal{T}_{\text{non-vac}}^{(a)\text{max}}$. We remark the increasing error of the approximate formulas in comparison with the exact formulas, observing that the error of $\mathcal{T}_{\text{non-vac}}^{(a)\text{max}}$ grows more rapidly.

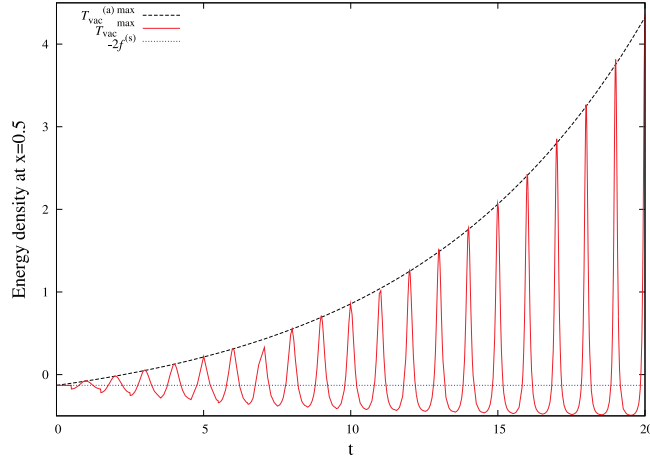


Figure 8: The energy density $\mathcal{T}_{\text{vac}}^{\text{max}}$ (solid line), given by Eq. (38), and its growing in time predicted by (40), for the case of $\epsilon = 10^{-2}$.

Table 1: $\mathcal{T}_{\text{vac}}^{\text{max}}$ and $\mathcal{T}_{\text{non-vac}}^{\text{max}}$ (for $T = 1$) computed via numerical exact method (column 2) and via approximate analytical formula (column 3), with $L_0 = 1$, $\epsilon = 10^{-2}$ and $p = 2$. The percent error $(\mathcal{T}_{\text{vac}}^{\text{max}} - \mathcal{T}_{\text{vac}}^{(a)\text{max}})/\mathcal{T}_{\text{vac}}^{\text{max}} \times 100$ is showed in column 4.

t	$\mathcal{T}_{\text{vac}}^{\text{max}}$	$\mathcal{T}_{\text{vac}}^{(a)\text{max}}$	Percent Error
10	0.864	0.856	0.870
10^2	115	113	2.16
5×10^2	0.832×10^{27}	0.761×10^{27}	8.44
10^3	0.175×10^{55}	0.148×10^{55}	15.7
	$\mathcal{T}_{\text{non-vac}}^{\text{max}}$	$\mathcal{T}_{\text{non-vac}}^{(a)\text{max}}$	
10	13.12	13.1	0.17
10^2	109×10^4	107×10^4	1.64
5×10^2	0.785×10^{28}	0.723×10^{28}	7.95
10^3	0.165×10^{56}	0.149×10^{42}	99.9

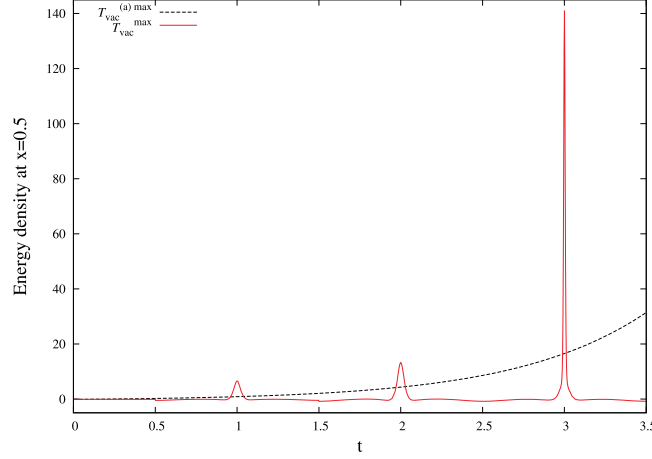


Figure 9: The energy density $\mathcal{T}_{\text{vac}}^{\text{max}}$ (solid line), given by Eq. (38), and its growing in time predicted by (40), for the case of $\epsilon = 10^{-1}$.

In Fig. 9 we examine the case discussed in Fig. 8, but with a larger amplitude: $\epsilon = 10^{-1}$. Now, we see disagreement between the maximum value of the energy density (38) and its growing in time predicted by (40). In Table 2, we examine the case discussed in Fig. 9, but for larger instants. We see large discrepancy between approximate and exact formulas.

In counterpart, if we diminish the amplitude to $\epsilon = 10^{-8}$, we get an excellent agreement between approximate and exact formulas for short and long times. For instance: $\mathcal{T}_{\text{vac}}^{\text{max}}(4 \times 10^4) \approx \mathcal{T}_{\text{vac}}^{(a)\text{max}}(4 \times 10^4) \approx -0.129$; $\mathcal{T}_{\text{non-vac}}^{\text{max}}(4 \times 10^4) \approx \mathcal{T}_{\text{non-vac}}^{(a)\text{max}}(4 \times 10^4) \approx 3.75$.

Table 2: $\mathcal{T}_{\text{vac}}^{\text{max}}$ and $\mathcal{T}_{\text{non-vac}}^{\text{max}}$ (for $T = 1$) computed via numerical exact method (column 2) and via approximate analytical formula (column 3), with $L_0 = 1$, $\epsilon = 10^{-1}$ and $p = 2$. The percent error $(\mathcal{T}_{\text{vac}}^{\text{max}} - \mathcal{T}_{\text{vac, non-vac}}^{(a)\text{max}})/\mathcal{T}_{\text{vac, non-vac}}^{\text{max}} \times 100$ is showed in column 4.

t	$\mathcal{T}_{\text{vac}}^{\text{max}}$	$\mathcal{T}_{\text{vac}}^{(a)\text{max}}$	Percent Error
10	191×10^4	113×10^3	94.1
40	0.338×10^{26}	0.266×10^{22}	99.9
	$\mathcal{T}_{\text{non-vac}}^{\text{max}}$	$\mathcal{T}_{\text{non-vac}}^{(a)\text{max}}$	
10	971×10^4	107×10^4	88.9
40	0.171×10^{27}	0.252×10^{23}	99.9

4. Conclusions

Considering a thermal bath as the initial field state in a cavity with a moving mirror in a two-dimensional space-time, we found for small amplitude of oscillation good agreement between the exact and approximate results for the maximum values of the energy densities. This agreement strengthens the validity of the analytical approximate results obtained in Ref. [18], and also reinforce the validity of the exact formulas and numerical results discussed here. However, for larger values of ϵ , as shown in Table 2, significant discrepancies appear. This is expected, since the analytical formulas are valid for $|\epsilon| \ll 1$. Then, we see that the exact formulas (22) and (23) can give results for cases of large amplitudes, which are out of reach of the perturbative approaches found in the literature.

We showed that the energy densities \mathcal{T}_{vac} and $\mathcal{T}_{\text{non-vac}}$ have, in general, different structures. However, we found that these energy densities can exhibit approximately the same structure for a class of laws of motion for which the ratio given in Eq. (34) is approximately a constant value. We also showed that this condition is just satisfied by the oscillating laws of motion with small amplitude investigated in the literature, specifically in Ref. [18], where the same structure for these energy densities was predicted via approximate methods. We verified that for this class of laws of motion there is a direct mapping between the approximate analytical formulas for the energy density found in the literature and the exact formulas discussed here. On the other hand, we found that for larger amplitudes of oscillation the ratio in Eq. (34) becomes far from a constant value, displaying larger oscillatory behavior. This means that that \mathcal{T}_{vac} and $\mathcal{T}_{\text{non-vac}}$ can display different structures. Moreover, the exact formulas (22) and (23) can say precisely how these structures are. Finally, we remark that, beyond the thermal case, the conclusions found in our letter are directly extensible to any other initial state whose density matrix is diagonal in the Fock basis.

Acknowledgements

We acknowledge the Referees for many constructive criticisms and suggestions to improve the final version of this letter. H.O.S. acknowledges the hospitality of Instituto de Física-UFRJ where part of this work was done. This work was supported by CNPq, CAPES and FAPESPA - Brazil.

References

References

- [1] G.T. Moore, J. Math. Phys. 11 (1970) 2679-2691.
- [2] S.A. Fulling, P.C.W. Davies, Proc. R. Soc. London A 348 (1976) 393-414.
- [3] P.C.W. Davies, S.A. Fulling, Proc. R. Soc. London A 356 (1977) 237-257.
- [4] B.S. DeWitt, Phys. Rep. 19 (1975) 295-357;
P.C.W. Davies, S.A. Fulling, Proc. R. Soc. London A 354 (1977) 59-77;
P. Candelas, D.J. Raine, J. Math. Phys. 17 (1976) 2101-2112;
P. Candelas, D. Deutsch, Proc. R. Soc. London, A 354 (1977) 79-99.

- [5] V.V. Dodonov, J. Phys.: Conf. Ser. 161 (2009) 012027-1-012027-28;
V.V. Dodonov, arXiv:1004.3301v1 (2010);
D.A.R. Dalvit, P.A. Maia Neto, F.D. Mazzitelli, arXiv:1006.4790v2 (2010).
- [6] C. Braggio *et al*, Europhys. Lett. 70 (2005) 754-760;
A. Agnesi *et al*, J. Phys. A: Math. Theor. 41 (2008) 164024-1-164024-7;
A. Agnesi *et al*, J. Phys.: Conf. Ser. 161 (2009) 012028-1-012028-7.
- [7] J.R. Johansson, G. Johansson, C.M. Wilson, F. Nori, Phys. Rev. Lett. 103 (2009) 147003-1-147003-4;
C.M. Wilson *et al*, arXiv:1006.2540v1 (2010);
J.R. Johansson, G. Johansson, C.M. Wilson, F. Nori, arXiv:1007.1058v1 (2010).
- [8] C.K. Law, Phys. Rev. Lett. 73 (1994) 1931-1934;
Y. Wu, K. W. Chan, M.C. Chu, P.T. Leung, Phys. Rev. A 59 (1999) 1662-1666;
P. Wegrzyn, J. Phys. B 40 (2007) 2621-2640.
- [9] V.V. Dodonov, A.B. Klimov, and D. E. Nikonov, J. Math. Phys. 34 (1993) 2742-2756.
- [10] D.A.R. Dalvit, F.D. Mazzitelli, Phys. Rev. A 57 (1998) 2113-2119.
- [11] C.K. Cole, W.C. Schieve, Phys. Rev. A 52 (1995) 4405-4415.
- [12] C.K. Cole, W.C. Schieve, Phys. Rev. A 64 (2001) 023813-1-023813-9.
- [13] L.H. Ford, A. Vilenkin, Phys. Rev. D 25 (1982) 2569-2575;
P.A. Maia Neto, J. Phys. A 27 (1994) 2167-2180;
P.A. Maia Neto, L.A.S. Machado, Phys. Rev. A 54 (1996) 3420-3427;
P.A. Maia Neto, L.A.S. Machado, Braz. J. Phys. 25 (1996) 324-334;
B. Mintz, C. Farina, P.A. Maia Neto, R.B. Rodrigues, J. Phys. A: Math. Gen. 39 (2006) 6559-6565;
B. Mintz, C. Farina, P.A. Maia Neto, R.B. Rodrigues, J. Phys. A: Math. Gen. 39 (2006) 11325-11333.
- [14] M. Razavy, J. Terning, Phys. Rev. D 31 (1985) 307-313;
G. Calucci, J. Phys. A 25 (1992) 3873-3882;
C.K. Law, Phys. Rev. A 49 (1994) 433-437;
V.V. Dodonov, A.B. Klimov, Phys. Rev. A 53 (1996) 2664-2682;
D.F. Mundarain, P.A. Maia Neto, Phys. Rev. A 57 (1998) 13791390;
D.T. Alves, C. Farina, E.R. Granhen, Phys. Rev. A 73 (2006) 063818-1-063818-8;
J. Sarabadani, M.F. Miri, Phys. Rev. A 75 (2007) 055802-1-055802-4.
- [15] M.-T. Jaekel, S. Reynaud, J. Phys. I (France) 3 (1993) 339-352;
M.-T. Jaekel, S. Reynaud, Phys. Lett. A 172 (1993) 319-324;
L.A.S. Machado, P.A. Maia Neto, C. Farina, Phys. Rev. D 66 (2002) 105016-1-105016-12;
D.T. Alves, C. Farina, P.A. Maia Neto, J. Phys. A 36 (2003) 1133311342;
D.T. Alves, E.R. Granhen, M.G. Lima, Phys. Rev. D 77 (2008) 125001-1-125001-5 .
- [16] V.V. Dodonov, J. Phys. A: Math. Gen. 31 (1998) 9835-9854;
G. Plunien, R. Schutzhold, G. Soff, Phys. Rev. Lett. 84 (2000) 1882-1885;
J. Hui, S. Qing-Yun, W. Jian-Sheng, Phys. Lett. A 268 (2000) 174-177;
R. Schutzhold, G. Plunien, G. Soff, Phys. Rev. A 65 (2002) 043820-1-043820-15;
G. Schaller, R. Schutzhold, G. Plunien, G. Soff, Phys. Rev. A 66 (2002) 023812-1-023812-20.
- [17] V.V. Dodonov, A. Klimov, V.I. Man'ko, Phys. Lett. A 149 (1990) 225-228;
D.A.R. Dalvit, P.A. Maia Neto, Phys. Rev. Lett. 84 (2000) 798-801;
V.V. Dodonov, M.A. Andreato, S.S. Mizrahi, J. Opt. B: Quantum Semiclass. Opt. 7 (2005) S468-S479.
- [18] M.A. Andreato, V.V. Dodonov, J. Phys. A 33 (2000) 3209-3223.
- [19] D.T. Alves, E.R. Granhen, H.O. Silva, M.G. Lima, Phys. Rev. D 81 (2010) 025016-1-025016-10.
- [20] www.maplesoft.com
- [21] D.T. Alves, E.R. Granhen, *The Dynamical Casimir package*, paper in preparation.